Faraday Discussions

Accepted Manuscript

This manuscript will be presented and discussed at a forthcoming Faraday Discussion meeting. All delegates can contribute to the discussion which will be included in the final volume.

Register now to attend! Full details of all upcoming meetings: http://rsc.li/fd-upcoming-meetings

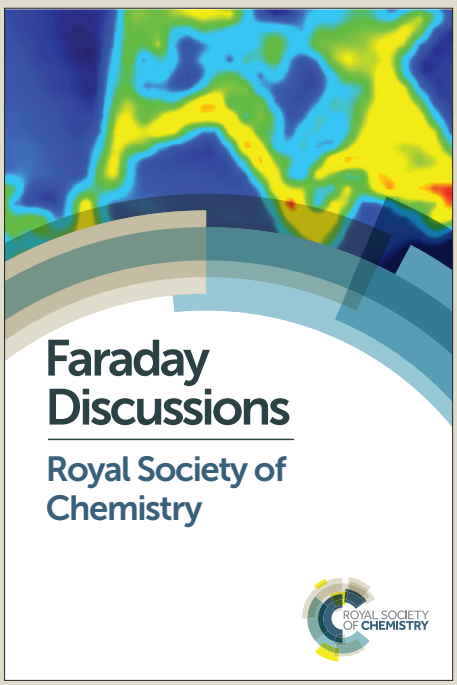

This is an *Accepted Manuscript*, which has been through the Royal Society of Chemistry peer review process and has been accepted for publication.

Accepted Manuscripts are published online shortly after acceptance, before technical editing, formatting and proof reading. Using this free service, authors can make their results available to the community, in citable form, before we publish the edited article. We will replace this *Accepted Manuscript* with the edited and formatted *Advance Article* as soon as it is available.

You can find more information about *Accepted Manuscripts* in the Information for Authors.

Please note that technical editing may introduce minor changes to the text and/or graphics, which may alter content. The journal's standard Terms & Conditions and the Ethical guidelines still apply. In no event shall the Royal Society of Chemistry be held responsible for any errors or omissions in this *Accepted Manuscript* or any consequences arising from the use of any information it contains.

ROYAL SOCIETY OF CHEMISTRY

www.rsc.org/faraday_d

Critical Importance of Gap Modes in Surface Enhanced Raman Scattering

Masayuki Futamata*, Maho Ishikura, Chiaki Iida, Saori Handa
Graduate School of Science and Engineering, Saitama University, Saitama 338-8570, Japan

Abstract

For efficient utilization of surface plasmons in surface enhanced Raman scattering (SERS), we investigated gap modes in flocculates of metal nanoparticles (MNPs), and between MNPs and metal substrates under an external and an attenuated total reflection (ATR) geometry. First, adsorbed state of thiol molecules and counter ions trapped in solutions were elucidated using flocculation-SERS, in which closely adjacent nanoparticles are formed by using interaction between MNPs and target species. Second, we obtained pronounced enhancement of 10^5-10^8 at a nanogap between gold nanoparticles (AuNPs) and various metal substrates even with large damping under an external geometry. Markedly larger enhancement was obtained for larger AuNPs, by a factor of 10^3 for particles with a radius (r) of 50 nm compared with those of r=15 nm in this geometry. Finally, we attained additional enhancement factor under an ATR geometry by a coupling of propagating surface plasmons with gap modes.

Introduction

Metal nanoparticles (MNPs) and metal nanostructures, which are precisely fabricated by top-down beam technologies and bottom-up chemical syntheses, have been utilized in surface enhanced Raman scattering (SERS). Marked enhancement in SERS, typically by a factor (G) of 10^4-10^6 in average, is arisen from specific electronic state in chemical enhancement (CE) mechanism and localized surface plasmons (LSPs) of metal nanostructures in electromagnetic (EM) enhancement [1]. In particular, surface plasmons are crucial to in situ characterizing individual molecules, because EM mechanism provides much larger enhancement ($G=10^4$-10^5 for isolated, and $G=10^8$-10^{10} for adjacent particles) irrespective of adsorbed species in contrast to CE mechanism ($G=10^2$-10^3) available only for specific molecules and vibrational modes. Even single molecule detection by Raman scattering has been reported at a nanogap of adjacent metal nanostructures (flocculates, intrinsically different from aggregates [2, 3]) by using a coupling of LSP resonances, which is one of gap modes (Fig. 1a).

To establish gap mode Raman spectroscopy using flocculated MNPs as an analytical tool, it is crucial to managing conflicting properties of surface residuals like citrates, which are electrostatic stabilization of MNPs in suspension, and steric hindrance for adsorption [4-9]. To overcome these issues, we exploited self-assembled monolayer (SAM) of thiol molecules here, which replaces surface residuals, and form flocculates of MNPs. In particular we focused ourselves on thiols having

functional groups, such as carboxylic and amino groups at solution side, to trap counter ions in solution. We have a plenty of reports on SERS of various SAM films on MNPs [11-15, 28], however, their detailed adsorbed states are still under discussion. For instance, photochemical reaction [11], and photo-induced charge transfer effect [12, 13] have been reported for p-aminothiophenol (PATP) on metal surfaces. Also, distinct adsorption features of p-mercaptobenzoic acid (PMBA) via S-M bonds or COO^- groups are reported on Ag and Au surfaces [15], which may affect pH sensing in living cell [14]. Thus, it is valid to investigate these PATP- and PMBA-SAM films on AgNPs using flocculation-SERS to characterize detailed adsorbed state and interaction with those on neighboring AgNPs and counter ions.

As the second geometry for the excitation of gap modes, MNPs/adsorbates/metal substrates have recently been developed [16-18], in which a coupling of dipoles in metal nanoparticles and image dipoles in metal substrates provides enormously enhanced electric field at a nanogap (Fig. 1b). In this geometry, various metal substrates are available including single crystals [18], and transition metal substrates with large damping [16, 17]. MNPs are efficiently immobilized on metal substrates via adsorbed molecules through van der Waals and electrostatic interaction [19]. Metiu et al. [20] analyzed enhanced electric field at a nanogap between MNPs and metal substrates in early ’80 with respect to the electromagnetic enhancement mechanism of SERS. Yet details in gap modes have not been reported, for instance how the enhancement factor depends on dielectric constants of substrates, and also on the size of MNPs. Here we investigated these issues using FDTD calculations and SERS measurements.

In the third configuration, gap mode plasmons are excited in an ATR geometry, in which AgNPs are attached to adsorbates on Ag film/prism. Propagating surface plasmons (PSPs) are excited at a resonance angle of incidence higher than the critical angle for total reflection, at which the wave vector and the energy of excitation light accord with those of PSPs at an Ag film/(molecules) air interface (Fig. 1c). The ATR configuration is promising in tip-enhanced Raman scattering (TERS) to suppress plausible background signal from sample illuminated with a laser spot (1-10 μm). Indeed, only an evanescent wave at sample surfaces, where the tip probe (with a size of 10-30 nm) approaches in TERS, is transferred to propagating light under an ATR geometry. However, the coupling of PSPs and gap modes has not been evaluated in detail. For instance it is not obvious if gap modes under an ATR geometry provide larger enhancement compared with an external geometry. Probably the excitation efficiency of PSPs is perturbed by AgNPs attached to Ag films/prism, and thereby related to sensitivity in TERS. We evaluated the SERS enhancement factor under PSP and gap mode excitation, using reflectivity and SERS measurements as well as with theoretical calculations, while varying surface coverage of AgNPs (θ_{AgNP}).

Thus, we investigated gap mode Raman spectroscopy in three distinct geometries such as flocculates of AgNPs, an external geometry for AuNP/adsorbates/metal substrates, and also an ATR configuration for AgNP/adsorbates/Ag films/prism to establish it as an analytical tool, while solving

their present issues.

Experimental setup

AgNPs and AuNPs were prepared by chemical reduction using trisodium citrate [4-8]. Sulfuric acid, sodium hydroxide, various thiol molecules were purchased from Wako Pure Chemicals, and used without further purifications.

(1) Flocculation SERS: p-aminothiophenol (PATP) and p-mercaptobenzoic acid (PMBA) molecules were adsorbed on AgNPs in aqueous solutions, whose pH values were adjusted between pH = 2-10 to protonate or deprotonate of thiol molecules by the addition of H_2SO_4 and NaOH. Here, pKa of an $-NH_3^+$ group in PATP and a –COOH group in PMBA in solutions is 6.9 and 5.9, respectively [8, 21].

(2) Gap modes under an external configuration: metal thin plates such as Sn, Zn, Pt, Pb, Cu and Al with sufficiently high purity (99.99- 99.999 %) were purchased from Nilaco Co., and used as substrates in gap modes. Self-assembled monolayers of thiophenol (TP) were formed on these metals [22] by immersing them in ethanol solutions of TP (1 mM) for 1 h, and rinsed with pure methanol to remove excess and uncombined thiol molecules, yielding TP-SAM on the above metal substrates. Then, a small amount of AuNP suspension (~100 μL with a density of ~10^{12} particles/mL) was dropped on TP-SAM coated metal substrates, and kept for 1 h to be immobilized through van der Waals interaction between TP, metal substrates and AuNPs [19]. Silicon wafers and cover glass slips were also used as substrates, which were immersed in p-styryl trimethoxy silane (PSTMS) in 2 % methanol solutions for 10 min followed by through rinsing with pure methanol, and by heating at 373 K for 10 min to polymerize PSTMS. Thus, a monolayer of PSTMS was formed on Si via Si-O-Si covalent bonds.

(3) Coupling of PSPs and gap modes in an ATR geometry: TP-SAM films were formed on Ag films (45 nm thickness) evaporated on a Dove prism, BK-7. AgNPs, on which residual citrates were replaced by Cl^-, were immobilized on TP-SAM/Ag films/prism substrates with a drop coating method.

An FDTD calculation was used to evaluate local electric field at a nanogap in three different geometries; (a) between AgNPs, (b) between AuNPs and various metal substrates under an external geometry, and (c) between AgNPs and Ag films on a Dove prism under an ATR geometry at various angles of incidence in 40-60° and at experimentally used excitation wavelengths of 632 nm (b) and 532 nm (c). Extinction spectra were measured to characterize the LSP resonance of isolated and flocculated AgNPs in solutions using a JASCO 540 uv-vis spectrophotometer. SERS spectra were measured for the sample solutions as those in extinction measurements, and also for AgNP/thiol-SAM/substrates under an external geometry (at an angle of incidence of 65°, with p-polarization) using a modified Renishaw micro-Raman spectrometer with a thin layer solution cuvette and a He-Ne laser (632.8 nm and <1 $\mu W/\mu m^2$). Also a Chromex polychromator (250is) equipped with a solid laser (532 nm, 20 mW) was used for SERS measurements of AgNP/thiol/Ag

film/prism samples under an ATR geometry. Surface coverage of AgNPs (θ_{AgNP}) as well as AuNPs, which was adjusted by dilution of as-prepared AgNP solutions from 1/1 to 1/200 in experiments (3), was evaluated by scanning electron microscope (SEM) images using Hitachi S-4100, as exemplified in Figs. 9a-9d. SERS enhancement factors at a nanogap in experiments (2) and (3) were estimated using θ_{AgNP} and by assuming SERS active area on metal substrates with a diameter of 1/5 of particles sizes, on the basis of enhanced electric field distribution obtained by FDTD calculations.

Results and Discussion

(1) Flocculation-SERS

AgNPs coated with PATP-SAM films feasibly formed flocculates when pH was not controlled [23]. Because pH in PATP solutions (10^{-4} M) used for SAM films formation is ~8.4, higher than pK_a of 6.85 for $–S-\phi-NH_3^+ \leftrightarrow -S-\phi-NH_2$, neutral PATP ($-NH_2$) species are predominant on AgNPs. Accordingly, van der Waals attractive potential, ~200 kJmol^{-1} [10], much larger than thermal energy 2.5 kJmol^{-1}, worked between neutral PATP-SAM films and AgNPs to form flocculates. In contrast, AgNPs coated with PATP-SAM remained isolated at pH~4, much lower than pK_a for $–NH_3^+$ in PATP, owing to electrostatic repulsion between protonated amino groups on neighboring AgNPs. This presumption was supported by the fact that flocculates of AgNPs (Fig. 2a) were formed by the addition of Na_2SO_4 (1 mM) or $HClO_4$ (5 mM). Accordingly, flocculates of AgNP-PATP$^+$…X^{n-}…$^+$PTAP-AgNP (here $X^{n+}=SO_4^{2-}$ or ClO_4^-) provided pronounced SERS spectra of trapped anions such as $\nu_{1S}(SO_4^{2-})$ band at 972 cm^{-1} and $\nu_{1S}(ClO_4^-)$ band at 931 cm^{-1}, in addition to SERS spectra from protonated PATP ($-NH_3^+$) ions. Concerning plausible photochemical reaction of PATP on Ag surfaces, we investigated SERS of PATP in flocculated AgNPs at different pH values. First, SERS spectra of PATP were observed on AgNPs at neutral pH (~7, Fig. 2b), which are significantly different from those of bulk powder of neutral PATP [23]. Prominent Raman bands were detected at 1572, 1420, 1378, 1187 and 1139 cm^{-1}, typical observed for PATP on Ag surfaces [11, 12]. Distinct SERS spectra from PATPH$^+$ ions with protonated amino groups ($-NH_3^+$) appeared in acidic pH solutions (~2<<pKa~5.8) at 1594, 1487, 1174, 1072, 975, 801, 630, and 393 cm^{-1} (Fig. 2b), which are similar to those for bulk state. These observations are consistent with those in previous reports [11, 12]. Note that SERS spectra of PATPH$^+$ molecules in acidic pH significantly changed by the addition of NaOH solutions, which increased pH to 10-11 higher than pKa. Indeed, new bands appeared at 1443, 1299, 1278, 1174, 851, 547, and 362 cm^{-1} in addition to invariable bands at 1594, 1072, 630 and 384 cm^{-1}(Fig. 2b). These SERS spectra obtained after the addition of NaOH solution are also significantly different from those prepared in neutral pH (Fig. 2b). The observed spectral changes are tentatively attributed to deprotonated PATP molecules, although we need further effort to draw conclusions while adjusting pH in solutions.

Next, PMBA with a carboxy group (-COOH), which was protonated in H_2SO_4 solution (pH=1-3 << pKa=5.5 of PMBA), caused flocculation of AgNPs (Fig. 3a) similar to the case for neutral PATP.

Interestingly, SERS spectra of PMBA adsorbed in a 1×10^{-6} M solutions, which yielded surface coverage of <0.1 monolayer (ML) as determined by a subtractive absorption method [8], are attributed to carboxylate anions ($-COO^-$). This assignment is validated by the observations of a pronounced broad peak at ~1380 cm^{-1} from a symmetric stretching mode ν_{sCOO-} of carboxylate anions ($-COO^-$), and also by no $\nu_{C=O}$ peaks at ~1700 cm^{-1} from carboxylic acid (-COOH, Fig. 3b). The Raman band intensity of ν_{sCOO-} at ~1380 cm^{-1} as well as those observed at 1132, 1004, 839, 711, and 357 cm^{-1}, which are assigned to vibrational modes of a deprotonated form of PMBA on Ag, decreased with increasing the concentration of PMBA from 1×10^{-6} (<0.1 ML) to 3×10^{-6} M (~0.1 ML) and 6×10^{-6} M (~0.25 ML). Concomitantly, $\nu_{C=O}$ peaks at 1705 and 1660 cm^{-1} in addition to those at 1291, 797, 689 and 323 cm^{-1}, which are assigned to those of protonated PMBA on AgNPs on the basis of DFT calculations, appeared at a concentration of PMBA higher than 3×10^{-6} M. Here, the broad Raman band at ~1380 cm^{-1}, observed at quite low coverage of PMBA, is attributed to carboxylate anions $-COO^-$ directly adsorbed on Ag surfaces with a flat or inclined orientation as suggested in literature [15]. Associating with this attribution, the addition of $MgCl_2$ (0.3 mM) to the acidic solution (pH=2) containing $PMBA^-$ anions adsorbed on AgNPs drastically decreased the intensity of the ν_{sCOO-} band at 1380 cm^{-1}, while increased that of $\nu_{C=O}$ band at 1700 and 1650 cm^{-1}. Probably, divalent cations Mg^{2+} flipped $PMBA^-$ anions with electrostatic interaction, of which $-COO^-$ anions facing to solution side resulted in protonation at pH<<pKa. At pH~12 (>>pKa), the corresponding sharp peak at 1430-1400 cm^{-1} from carboxylate anions facing to solution side showed significant shift (20-30 cm^{-1}) by addition of different metal ions [8]. Thus, slightly higher coverage of PMBA between 0.1~0.25 ML changed its orientation from flat or inclined to vertical to the surface of AgNPs with the $-COO^-$ group facing to solution side. Such orientation change was probably caused by markedly lower surface pH in addition to larger molecular interaction at higher coverage. Interestingly, PMBA-coated AgNPs again isolated at much higher coverage of ~1 ML in pH=2 as evidenced by a single extinction peak at ~420 nm from isolated AgNPs (Figs. 2a and 3a). If surface residual of citrate ions on AgNPs are thoroughly replaced with PMBA, AgNP should immediately form flocculates or aggregates due to van der Waals attractive force. Hence, the re-isolation at ~1 ML in acidic condition, pH(2)<<pKa(5.8), is probably caused by citrates partly remaining on AgNPs, to which ion pair formation of hydrated proton is sterically hindered by densely packed PMBA-SAM films. This is in contrast to those observed at lower surface coverage (0.1 – 0.25 ML), at which hydrated protons are feasibly located nearby surface citrates to neutralize their charges. These presumptions were supported by significantly negative zeta potential (ca. -20 mV) of AgNPs observed at ~1 ML coverage of PMBA in acidic conditions, while the potential value is much smaller than that (ca. -45 mV) observed for as-prepared AgNPs. In an alternative way for the protonation, AgNPs adsorbed by $PMBA^-$ anions at pH=5-6 in 3×10^{-6} - 6×10^{-5} M solutions flocculated after the addition of H_2SO_4 (1-10 mM), which decreased pH to 1-3. In this case, SERS spectra were obtained not from $PMBA^-$ anions with $-COO^-$ groups facing to AgNPs, but

only from protonated PMBA molecules (Data not shown). These distinct features of protonation and deprotonation of PMBA on AgNPs are due to preferential adsorption via carboxylate groups at low surface coverage in acidic conditions and those via thiol groups in neutral pH. In addition, we confirmed that carboxy groups in PMBA adsorbed in flocculates of AgNPs are almost reversibly protonated and deprotonated by tuning pH in solutions (Fig. 4).

Thus, we found the crucial role of van der Waals and electrostatic interaction in flocculation of AgNPs, which facilitates to characterize adsorbed state of various species. Complicated adsorbed state of PATP- and PMBA-SAM films on AgNPs, and their interaction with counter ions were elucidated at different pH values.

(2) Gap mode-SERS under an external geometry.

2.1) FDTD calculations

A gap mode resonance occurred at ~550 nm for AuNPs (r=15 nm), with a gap size of 1 nm, on various metal substrates such as Ag, Cu, Zn, Pt, Pb, Sn, and Al irrespective of their distinct optical properties. Enormous enhancement factors of 2.5×10^3-1.0×10^4 were obtained in electric field at a nanogap, which was normalized to that in an incident light ($|E_{gap}/E_{in}|^2$, Figs. 5a-5b and Table 1). The larger size of AuNPs yielded the larger enhancement factor. For instance, the enhancement factor of 5.2×10^3 for r=15 nm at a resonance wavelength of ~550 nm increased to 3.8×10^4 for r=50 nm at resonance wavelengths of ~660 nm on Zn and Sn (Fig. 6a, Table 1), which roughly provides Raman enhancement factor of ~1.4×10^9. Gold spherical particles with a size (r) larger than 50 nm yielded almost identical enhancement to that for r=50 nm, for example 1.3×10^5 (1.6×10^5) for r=100 nm (r=50 nm) on Cu substrate, while resulting in wider resonance widths (FWHM) from 120 nm (for r=50 nm) to 250-300 nm (for r=100 nm) (Fig. 6a). Thus, gap mode Raman spectroscopy can be applied to various metal substrates even with large damping, which is given by the ratio of a real part (ε_r') to imaginary part (ε_{im}") of optical constants ($\varepsilon_{metal} = \varepsilon_r' + i\,\varepsilon_{im}"$). For instance, magnitude of enhanced electric field on metal substrates under the resonance of propagating surface plasmons is proportional to $|\varepsilon_r'|^2/\varepsilon_{im}"$, which is 596 (Ag), 82.7 (Au), 53.9 (Cu), 15.0 (Zn), and 6.79 (Pt), 5.16 (Pb) at ~610 nm. It reminds us that only coin metals like Ag, Au and Cu are utilized as SERS active substrates on the basis of their high efficiency in exciting localized surface plasmons on roughened surfaces. Nevertheless, gap mode Raman spectroscopy is capable of elucidating catalytic reaction on transition metals like Pt [10, 11], Fe [19] or detailed adsorbed states on distinct atomically smooth surfaces of Au single crystals [18].

Marked enhancement of electric field at a nanogap is rationalized by a mechanism underlying in gap modes. Localized surface plasmons in AuNPs excited by a laser illumination form oscillating dipoles (*p*) or multipoles in AuNPs at a resonance wavelength slightly modified by the presence of metal substrates. These dipoles or multipoles induce image dipoles (*p'*) or multipoles in metal substrates, which are located in close vicinity of AuNPs, as given by Eq. 1 [24].

$$p' = \frac{\varepsilon_{sub} - \varepsilon_{med}}{\varepsilon_{sub} + \varepsilon_{med}} p \quad .....(1)$$

Here, ε_{sub} and ε_{med} are optical constants of metal substrates and surrounding media, respectively. These dipoles and image dipoles couple to form enhanced electric field at a nanogap [25]. To ensure this mechanism, we calculated a gap mode resonance and enhanced electric field for an AuNP/gap/Al sample, while changing a gap size between 1-20 nm. As shown in Fig. 6b, an LSP resonance for an isolated AuNP at ~530 nm only slightly modified to a gap mode resonance at ~560 nm with decreasing a gap size, in particular between 5 nm and 1nm, proving a predominant role of LSPs. Note that sufficiently large oscillating dipoles, which are similar to those in flocculates of AuNPs, are induced in various metal substrates, because optical constant of metals is in general much larger than that of media. Indeed, optical constants of Pt, $\varepsilon_{sub(Pt)}$ = -11.3+i18.7 [26] is much larger than that of media, air (ε_{med}=1) in our experiments, yielding $|p'|^2$=1.1× $|p|^2$ as summarized in Table 1. Even virtual metals with a small real part and extremely large imaginary part like ε_{sub} =-1.0+i100, corresponding to $|p'|^2$ = 1.0×$|p|^2$, yielded 10^3-10^4 of enhancement factor in electric field intensity. Consequently, metal nanoparticles, here AuNPs, determine the gap mode resonance and enhancement factor at a nanogap via the LSP resonance (Table 1). Indeed, pronounced enhancement factors in Raman scattering for various metal substrates were experimentally confirmed as described in Section 2.2.

In addition, these results suggest not only metals but also dielectric substrates with enough large optical constants, such as silicon (ε_{Si}= 15.5+i0.20 at 600 nm [26]) are available in gap mode Raman spectroscopy. Silicon substrate indeed provided pronounced enhancement factor of 1.4×10^4 (Si) in electric field at a nanogap at a resonance wavelength of ~610 nm, compared with much modest value (2.3×10^2) for BK-7 ($\varepsilon_{BK\text{-}7}$=2.10 at 600 nm) as shown in Fig. 7a. Accordingly, enhancement factor in Raman scattering predicted for Si substrate is much larger than that for cover slips (BK-7). This calculation was experimentally assured in section 2.2. Thus, relevance of gap mode Raman spectroscopy was anticipated not only for largely damping metals but also for dielectric materials with sufficiently large optical constants.

We also corroborated that markedly enhanced electric field is formed at nanogaps in flocculated of MNPs by a coupling of dipoles and image dipoles in neighboring MNPs. In particular, an MNP with smaller damping like Ag and Au induces sufficiently large image dipoles in a closely adjacent MNP with larger damping such as Pt and Vi (Virtual metal with ε=-1+i100). Indeed, enhancement factors in electric field intensity for these heterogeneous pair of particles (with r=30 nm and a gap size of 1 nm), such as 2.0×10^4 for AuNP-PtNP and 2.3×10^4 for AuNP-ViNP at their resonance wavelengths (550-600 nm), are comparable with those for AuNP-AuNP (1.7×10^5) and AgNP-AgNP (6.2×10^5). These enhancement factors are significantly larger than those anticipated for homogeneous pair of MNPs with large damping like PtNP-PtNP (3.1×10^3) and ViNP-ViNP (1.8×10^3, Fig. 7b). Inherently the same results were obtained for MNPs on metal substrates. For instance, rather modest enhancement in electric field is formed at a nanogap between MNPs and metal substrates like AlNP-Al substrate

(2.4×10^3) and PtNP-Pt substrate (1.8×10^3) both with large damping at ~600 nm.

2.2) Experimental observations

First, we found that all the metal substrates used here, Au, Ag, Pb, Pt, Sn, Cu, Al and Zn provided pronounced Raman spectra (Figs. 8a-8e) and similar enhancement factors of 10^5-10^6 for TP molecules (Table 1), when a He-Ne laser illuminated AuNPs (r~15 nm) immobilized on TP-SAM films on these metals. Essentially the same Raman spectra having identical peak positions and peak landscapes were observed for all the substrates used. These are also similar to those observed for bulk liquid TP under the same geometry with the micro Raman equipment. These observations suggest vertical or slightly tilted orientation of TP bound to these metal substrates via an S-Au bond, where in-plane modes are preferentially enhanced compared with out-of-plane modes. Since almost no Raman signals were detected without AuNPs on these samples, gap modes between AuNPs and metal substrates provide marked enhancement in electric field at a nanogap. Here, the enhancement factors were estimated for a gap region approximated to a disc on metal substrates with a radius of 3 nm under AuNPs (r=15 nm), where remarkably enhanced electric field is centered [4]. In this estimation, SEM images of each sample of AuNP/TP/metal substrates were observed to evaluate the number of AuNPs immobilized on metal substrates via TP-SAM molecules, as exemplified in Figs. 9a-9d. Apparently, quite similar enhancement factors in Raman scattering were obtained for different metal species as anticipated by theoretical calculations, ensuring predominant role of AuNPs to a gap mode resonance. These Raman enhancement factors observed for the immobilization of AuNPs are obviously not as large as those (10^8-10^9) for AgNPs [21]. However, this difference is not essential but primarily originated from distinct sizes of used AgNP and AuNP, namely r=30 nm (AgNPs) and r=15 nm (AuNPs). Indeed, the larger enhancement factors of 10^8-10^{10} were obtained for the larger AuNP like r=30-50 nm by FDTD calculations (*vide supra*, Fig. 6a, Table 1). We experimentally confirmed that larger size of AuNPs provided larger enhancement, such as 9.8×10^6 for r=50 nm compared with 1.3×10^6 for r=15 nm on Zn substrates (Fig. 8d). Essentially similar results for larger AuNPs were obtained on Cu substrates (Table 1). Potentially, single molecule detection can be achieved by using appropriate size of AuNPs on various metal substrates.

Second, we applied gap modes to dielectric substrates such as Si wafer and glass cover slip (BK-7) to ensure predicted results by FDTD calculations, which also pertains to an enhancement mechanism of gap modes. As described in experimental sections, PSTMS monolayers were formed on these substrates followed by immobilization of AuNPs with van der Waals interaction. As shown in Figs. 8f, Si substrates provided sufficiently large enhancement in Raman scattering of PSTMS, whereas much weaker Raman signal intensity was obtained for the same samples on cover glass after immobilization of AuNPs. Empirical enhancement factor for Raman scattering of PSTMS on Si under a gap mode resonance was estimated to be 1.7×10^6 using a Raman band at 1181 cm^{-1}. Thus, we found that gap mode Raman spectroscopy can be extended even to dielectric substrates with large optical constants.

(3) A coupling of PSPs and gap modes under an ATR configuration

The resonance angle for PSP excitation was observed to be ~43.6° at 532 nm with p-polarization for TP-SAM/Ag film (45 nm)/BK-7 prism in air, which was in good agreement with the theoretical value of 43.2° (Data not shown). Raman enhancement factor for TP band at 1069 cm^{-1} (ν_{C-S}) was estimated to be 7×10^3, which corresponds well to those 2.2×10^4 predicted by theoretical calculations (Table 2). The observation that s-polarized light did not give any reflectivity dip or Raman enhancement in contrast to p-polarization enabled us to conclude the above observations were caused by the excitation of PSPs. Immobilization of AgNPs to TP-SAM/Ag film/prism samples with θ_{AgNP}~0.7 % (Table2, see also Figs. 10a-10d and 11a-11d) slightly shifted the resonance angle to 44.3°, and provided much larger Raman enhancement of 2.6×10^5, which resulted from an excitation of gap modes in addition to PSPs. The surface coverage of AgNPs was empirically determined by SEM measurement as described in Section 2.2. The above enhancement factor is an averaged value over entire Ag films illuminated by a laser spot. The actual enhancement factor for thiol molecules at a nanogap was estimated to be 1.3×10^9 on the basis of the surface coverage (~0.7 %) of AgNP and active area ($4\pi r^2=4\pi\times4^2\sim$ 200 nm^2 under each AgNP) of the gap mode. The empirical enhancement in an ATR geometry (1.3×10^9), which corresponded to that (5.6×10^{11}) for AgNP/gap (1 nm)/Ag (45 nm)/prism samples anticipated by the FDTD calculations, was significantly larger than that obtained in an external geometry (9×10^7). We also noted that larger surface coverage of AgNPs gave higher averaged Raman intensity, but significantly smaller enhancement factor at the nanogap (Table 2). For instance, we obtained experimental (calculated) enhancement factor of 1.3×10^9 (5.6×10^{11}), 1.2×10^8 (9.4×10^{11}) and 2.4×10^7 (8.8×10^9) for surface coverage of AgNPs (θ_{AgNP}) of 1, 3 and 10 %, respectively (Figs. 10a-10d and 11a-11d). Probably, smaller enhancement at higher θ_{AgNP} results from less efficient excitation of the PSPs. Indeed, lager number of AgNPs increased scattered light intensity above a prism, which decreased evanescent field intensity on Ag films, as observed for roughened Ag films [27]. Lower excitation efficiency of PSPs was convinced by shift in the resonance angle from 43.2° to higher angle of incidence, 44.5°, 46.0° and 54.0° with larger width of 1, 1.5 and 4.0 ° for the surface coverage of AgNPs of 1, 3 and 10 %, respectively. These observations indicate larger damping of PSP field at higher θ_{AgNP}, which correspond well with the experimental observations (Table 2). In TERS measurements, only one AgNP attached on the tip of a cantilever does not perturb PSP resonances and thus provides the largest enhancement in electric field at a nanogap.

Gap modes combined with PSPs provided Raman enhancement of 9×10^{11} at 532 nm (slight off-resonance), which is comparable with those of 5×10^{12} at the resonance wavelength of 470 nm. These values are significantly larger than those predicted for gap modes under an external geometry, such as 2×10^8 at 532 nm and 6×10^{10} at 470 nm. These differences were attributed to the fact that PSPs are efficiently excited at much wider wavelength than gap modes [27]. Indeed, only slight shift of the

resonance angle for PSPs was observed from 44.8° at 470 nm to 43.2 ° at 532 nm, which provided equivalent evanescent field in proximity of Ag films. This evanescent field is similarly enhanced by a factor of ~10^2 at these wavelengths relative to incident light intensity, which assures significantly larger enhancement when coupled with gap modes in an ATR geometry compared to that in an external geometry.

Conclusions

Gap modes in flocculates of MNPs, and between MNPs and metal substrates under external and ATR configurations were investigated to establish them as an analytical tool. We succeeded to form flocculates of AgNPs using electrostatic interaction between dissociated PMBA ($-COO^-$), protonated PATP ($-NH_3^+$) and counter ions (M^{n+}, X^-), as well as using van der Waals force between neutral PMBAs (-COOH) and PATP ($-NH_2$) on AgNPs. Detailed adsorbed state of PMBA and PATP as well as trapped counter ions, depending on surface coverage and pH in solutions, was elucidated using enormous SERS enhancement. In gap modes under an external geometry, we found that various metal substrates with large damping including Pb, Sn, Cu, Zn, Al, and Pt are available. Note that these metal substrates, which were not effective in early stage of SERS history using their roughened surfaces, provided markedly enhanced electric field of 10^5-10^7 at a nanogap against AuNPs (r=15 nm). These features are explained by a coupling of dipoles in AuNPs and their image dipoles in the substrates. Hence, not only metal substrates but also dielectrics with large optical constants, such as Si with dielectric constants larger than 10 at 632 nm, relative to that of surrounding media provided pronounced enhancement (~10^6) in SERS. The larger size of AuNP provided the larger enhancement in electric field at a nanogap, for instance enhancement in the electric field from 5.2×10^3 (at r_{AuNP}= 15 nm) to 3.8×10^4 (at r_{AuNP}=50 nm) on Zn substrate, yielding 10^8-10^{10} of SERS enhancement on various metal substrates as experimentally supported. In gap modes under an ATR configuration, we corroborated by FDTD calculations and SERS measurements that additional enhancement is obtained by a coupling of PSPs and gap modes. Furthermore, a larger enhancement factor is provided at lower surface coverage of AgNPs due to more efficient excitation of PSPs, suggesting the highest enhancement in tip-enhanced Raman scattering.

Acknowledgement

This research was supported by KAKENHI (25286014 and 25600022) by JSPS. M.F. appreciates Prof. Mitsuru Ishikawa (Josai University) for useful discussions. The authors thank to Shin-Etsu Chemical Co. Ltd. for their kind supply of PSTMS.

References

(1) A. Otto, I. Mrozek, H. Grabhorn, W. Akemann, J. Phys. Condens. Matter 4 (1992) 1143-1212.

(2) K. Kneipp, M. Moskovic, H. Kneipp (eds.), "*Surface Enhanced Raman Scattering*", Springer, Berlin, 2006.

(3) E. C. Le Ru, P. G. Etchegoin, "*Principles of Surface-Enhanced Raman Spectroscopy*", Elsevier, 2009.

(4) M. Futamata, Y. Yu, T. Yanatori, T. Kokubun, *J. Phys. Chem. C*, **114**, 7502 (2010).

(5) T. Yajima, Y. Yu, M. Futamata, *Phys. Chem. Chem. Phys.* **13**, 12454 (2011).

(6) M. Futamata, Y. Yu, T. Yajima, *J. Phys. Chem.* C **115**, 5271 (2011).

(7) T. Yajima, Y. Yu, M. Futamata, *J. Raman Spectrosc.* **44**, 406 (2013).

(8) Y. Yu, S. Handa, T. Yajima, M. Futamata, *Chem. Phys. Lett.* **560**, 49 (2013).

(9) S. Handa, Y. Yu, M. Futamata, *J. Surf. Sci. Soc. Jpn.*, 34 (2013) 449-454.

(10) J. N. Israelachvili, "*Intermolecular and Surface Forces*", Academic Press, London, 1991.

(11) L.-B. Zhao, M. Zhang, Y.-F. Huang, C. T. Williams, D.-Y. Wu, B. Ren, Z.-Q. Tian, *J. Phys. Chem. Lett.* 2014, 5, 1259−1266 and references therein.

(12) K. Kim, K. L. Kim, K. S. Shin, *J. Phys. Chem. C*, 117 (2013) 5975-5981 and references therein.

(13) M. Osawa, N. Matsuda, K. Yoshii, I. Uchida, *J. Phys. Chem.* 98 (1994) 12702-12707.

(14) J. Kneipp, H. Kneipp, B. Wittig, K. Kneipp, *J. Phys. Chem. C* 114 (**2010)** 7421-7426.

(15) A. Michota, J. Bukowska, *J. Raman Spectrosc.* 34 (2003) 21.

(16) Z. Liu, S-Y. Ding, Z-B. Chen, X. Wang, J-H. Tian, J. R. Anema1, X-S. Zhou, D-Y. Wu, B-W Mao, X. Xu, Bin Ren, Z-Q. Tian, *Nature Commun.* 2 (2011) 305.

(17) K. Kim, H. B. Lee, J-Y. Choi, K. S. Shin, *J. Phys. Chem. C*, 115, 21047 (2012).

(18) K. Ikeda, K. Takahashi, T. Masuda, H. Kobori, M. Kanehara, T. Teranishi, K. Uosaki, *J. Phys. Chem.* 116, 20806-20811 (2012).

(19) H. Suzuki, H. Chiba, M. Futamata, *Vib. Spectrosc.* 72 (2014) 105-110.

(20) P. K. Aravind, H. Metiu, *Surf. Sci.* 124 (1984) 506.

(21) F. Raulin, J-P. Lussiana, *Origins of Life*, 14 (1984) 157.

(22) J. C. Love, L. A. Estroff, J. K. Kriebel, R. G. Nuzzo, and G. M. Whitesides, *Chem. Rev.* 105 (2005) 1103-1169.

(23) S. Handa, Y. Yu, M. Futamata, *Vib. Spectrosc.* 72(2014)128-134.

(24) T. Okamoto, I. Yamaguchi, *Opt. Rev.* 6 (1999) 211-214.

(25) J. D. Jackson, "*Classical Electrodynamics*", Second Ed., John Wiley & Sons (1975) Chap. 2.

(26) D. Palik, "*Handbook of Optical Constants of Solids*", Academic press (San Diego) 1998, pp. 333, 547 and 795.

(27) H. Raether, "*Surface Plasmons*", Springer Berlin 1988.

(28) C. E. Talley, L. Jusinski, C. W. Hollars, S. M. Lane, T. Huser, *Anal. Chem.* 76 (2004) 7064-7068.

Table 1 Enhancement factor for SERS signal intensity of TP under a gap mode resonance

Substrate materials	Observed (λ_{ex}=633 nm)	Calculated (λ=617 nm)
Ag(r_{AuNP}=15 nm)	1.6×10^{6}	1.3×10^{7}
Ag(r_{AuNP}=50 nm)	1.3×10^{8}	1.0×10^{10}
Cu(r_{AuNP}=15 nm)	3.3×10^{5}	5.3×10^{7}
Cu(r_{AuNP}=50 nm)	3.4×10^{7}	1.2×10^{10}
Zn (r_{AuNP}=15 nm)	1.3×10^{6}	2.3×10^{6}
Zn (r_{AuNP}=50 nm)	9.8×10^{6}	1.3×10^{9}
Pb	1.5×10^{5}	8.1×10^{6}
Sn	1.1×10^{6}	3.4×10^{6}
Pt	1.2×10^{6}	2.3×10^{6}
Al	2.6×10^{6}	2.8×10^{6}
Si*(r_{AuNP}=50 nm)	1.7×10^{6}	6.1×10^{7}
SiO_2(r_{AuNP}=50 nm)	$<<10^{6}$	5.1×10^{4}

*In calculation on Si substrate, naturally oxide layer (SiO_2, ~1 nm) was assumed.

Table 2 Resonance conditions and enhancement factor for PSPs coupled with gap modes

	θ_{AgNP} (%)	θ_{PSP} (°)	FWHM (°)	Enhancement (gap, G_{gap})	Enhancement (averaged, G_{av})
Calcd.	0	43.2	0.4	-	3.3×10^{4}
	1	44.5	1	5.6×10^{11}♣	-
	3.1	46.0	1.5	9.4×10^{11}♣(4.9×10^{9}♦)	-
	5.6	47.5	2.8	3.6×10^{10}	
	13	54.0	4	8.6×10^{9}♣	-
Obsd.	0	43.6	1.3	-	7×10^{3}
	0.7	44.3	1.6	1.3×10^{9}*	2.6×10^{5}
	1.4	44.0	1.4	1.8×10^{8}*	2.1×10^{5}
	2.8	45.0	2.2	1.2×10^{8}*	2.7×10^{5}
	4.6	44.3	2.9	3.7×10^{7}*	7.7×10^{5}
	10.6	44.0	4.1	2.4×10^{7}*	2.1×10^{5}
	17.6	45.0	5.3	6.8×10^{6}*	1.4×10^{5}
	25	47.7	>6	2.9×10^{6}*	2.1×10^{5}

*Enhancement in Raman scattering at a nanogap (G_{gap}) estimated from observed enhancement factor averaged (G_{av}) for entire Ag films by using $G_{av}\times\{(r/r_{ac})^2/(\theta_{AgNP})\}$. Here, r and r_{ac} denote averaged radii of AgNPs and active area under each AgNP, respectively. The Raman band of TP at ~1069 cm^{-1} ($\nu_{C\text{-}S}$) was employed in evaluation of the enhancement. The size of active area under each AgNP roughly corresponds to ~r/5 of AgNP.

♣Enhancement in Raman scattering estimated by FDTD calculations by using $|E_{gap}/E_0|^4$. Here, E_{gap} and E_0 denote electric field amplitude at a nanogap and incident light, respectively.

♦Enhancement in Raman scattering at a nanogap under an external geometry.

Figure captions

Fig. 1 Three distinct gap mode geometries: (a) in flocculation of MNPs, (b) under an external geometry, (c) in TERS under an ATR geometry.

Fig. 2 Extinction spectra (a) and SERS spectra (b) of flocculates of PATP on AgNPs adsorbed at different pH (see the text in detail).

Fig. 3 SERS spectra of flocculates of PATP adsorbed AgNPs in acidic condition at different coverage of PATP (θ): (a) θ<0.1 ML (1×10^{-6} M), (b) θ=0.1 ML (3×10^{-6} M), (c) θ=0.25 ML (6×10^{-6} M).

Fig. 4 SERS spectra of flocculates of AgNPs covered with protonated PMBA (a, c) and deprotonated PMBA (b, d). Sulfuric acid wad added before (a, c) and after (b, d) adsorption of PMBA on AgNPs.

Fig. 5 A gap mode resonance and enhanced electric field intensity for AuNP(r=15 nm)/gap (1nm)/metal (M) substrates, here M=Pb, Cu, Sn, Zn and Pt, calculated with an FDTD method: (a) at various excitation wavelengths, (b) spatial distribution at a nanogap.

Fig. 6 Local electric field amplitude ($|E_{gap}/E_{in}|$) at a nanogap for AuNP/ gap (G)/metal (M) substrates under a gap mode resonance: (a) as a function of size of AuNPs (r=radius) for M=Ag, Cu, Zn and Al with G=1 nm, and (b) as a function of gap size for r=30 nm.

Fig. 7 A gap mode resonance and enhanced electric field calculated with an FDTD method: (a) for AuNP(r=15 nm)/gap (1nm)/dielectric (D) substrates, here D=Si, and SiO_2, and (b) for flocculates of MNPs, here MNP=Au, Pt, Al, and virtual metal (VM, ε=-1+100i).

Fig. 8 Raman spectra of TP in AuNP/TP-SAM/metal substrates (M) under an external geometry: (a) M=Pb (a), Cu(b), Sn (c), Zn (d)$^{+}$, Pt (e) and Si (f)*. $^{+}$ The effect of AuNP size, r_{AuNP}=15, 25 and 50 nm, on enhancement was measured for Zn substrate. *PSTMS-SAM films were formed on Si instead of TP-SAM films in Figs. 8 and 9.

Fig. 9 SEM images of AuNP immobilized on different substrates via TP-SAM films: (a) on Cu, (b) on Cu (with different magnification), (c) on Sn, and (d) on Si* substrates.

Fig. 10 Calculated ATR reflectivity at different coverage (θ) of AgNPs in AgNPs/TP-SAM/Ag film (45 nm)/prism: (a) θ=1, (b) θ=3.1, (c) θ=5.6, and (d) θ=13 %.

Fig. 11 Experimental ATR reflectivity at different coverage (θ) of AgNPs in AgNPs/TP-SAM/Ag film (45 nm)/prism: (a) θ=1.4, (b) θ=2.8, (c) θ=4.6, and (d) θ=10.6 %.

Fig. 12 Raman spectra at different angles of incidence for AgNPs (θ=2.8 %)/TP-SAM/Ag film (45 nm)/prism.

Fig. 1a-1c

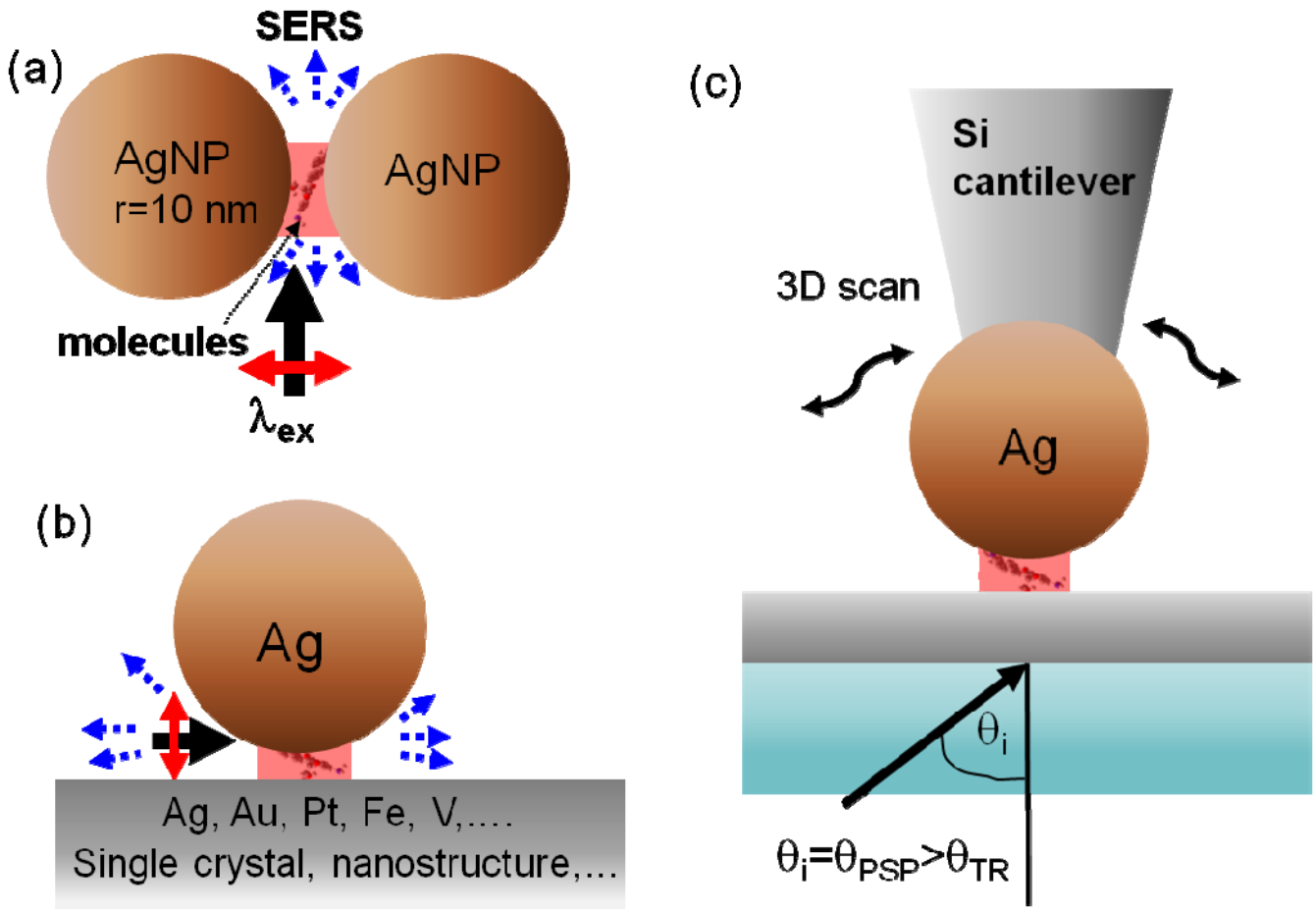

Fig. 2a-2b

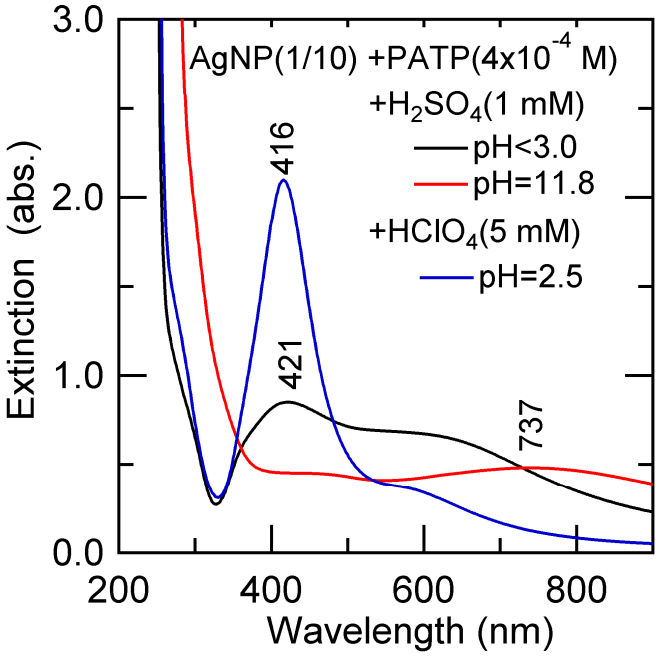

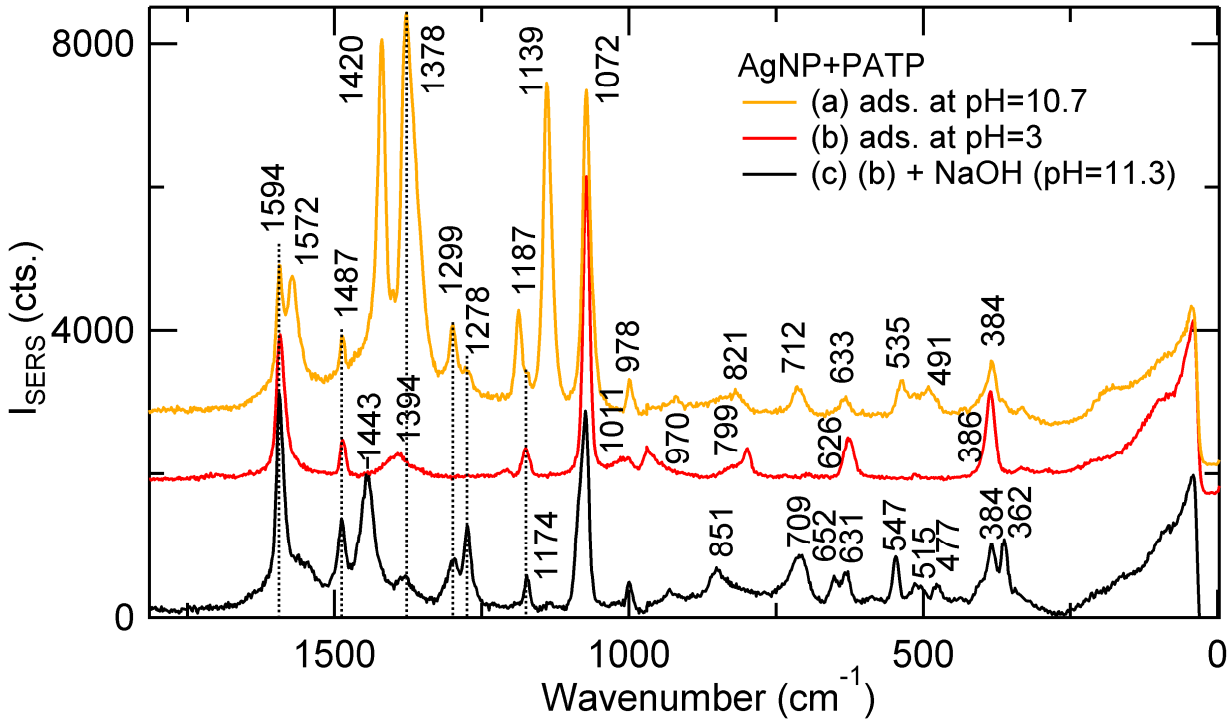

Fig. 3a-3b

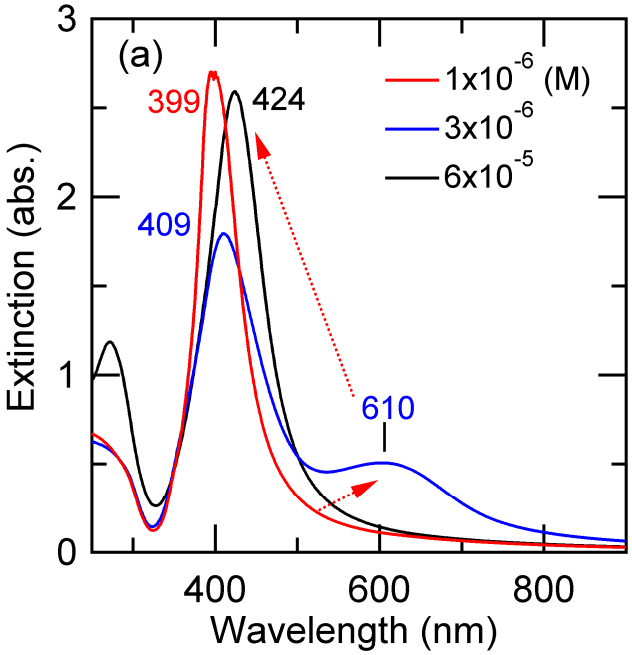

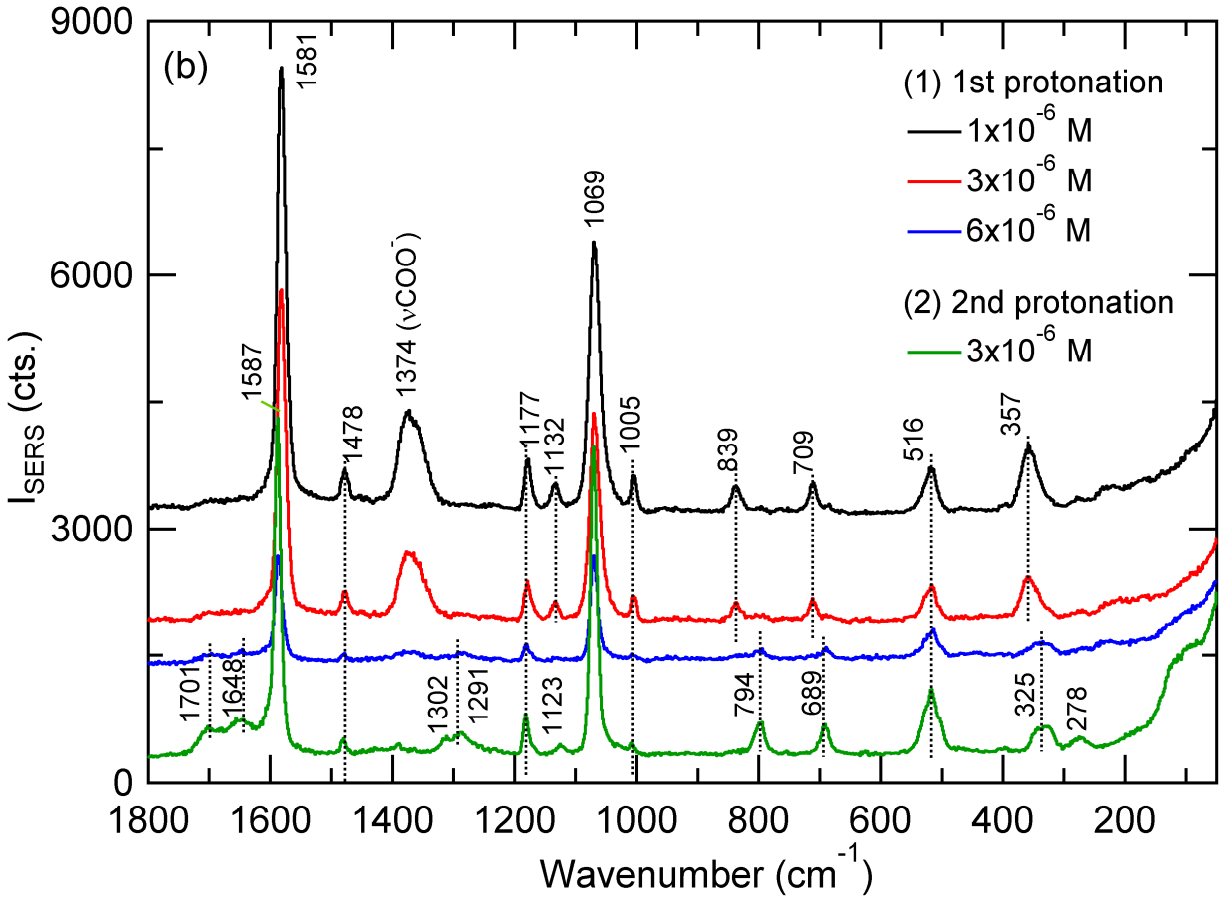

Fig. 4

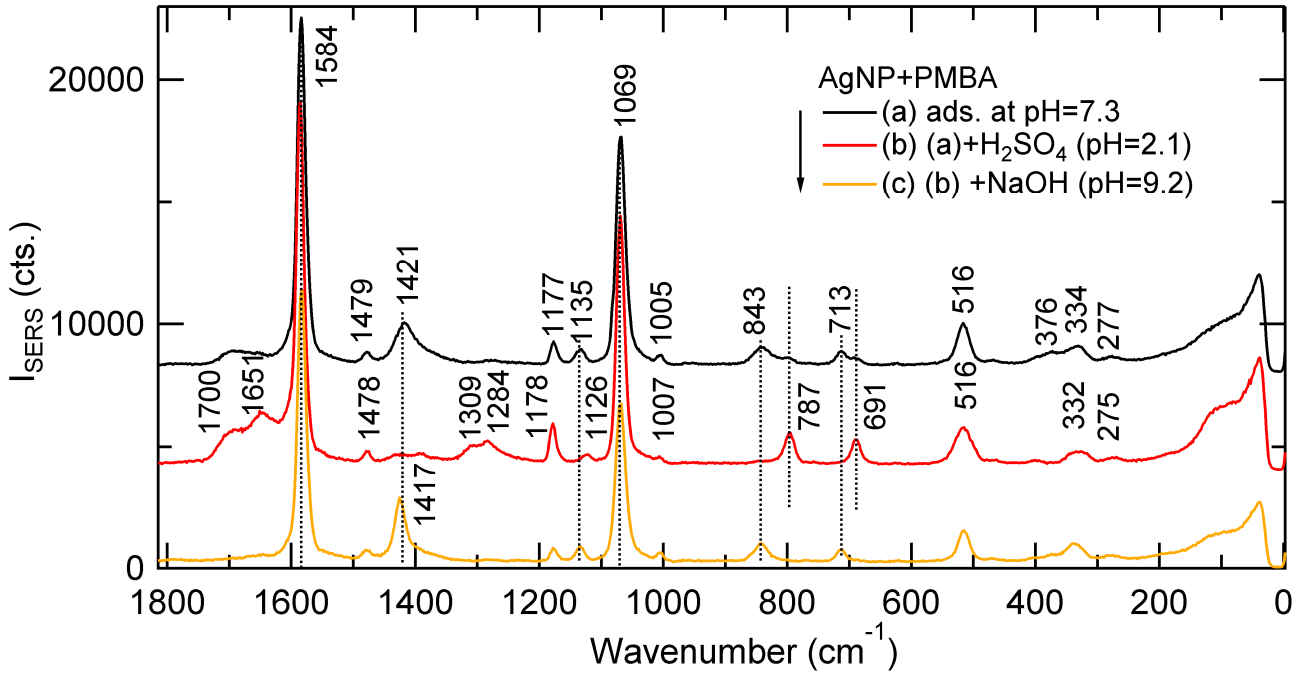

Fig. 5a-5b

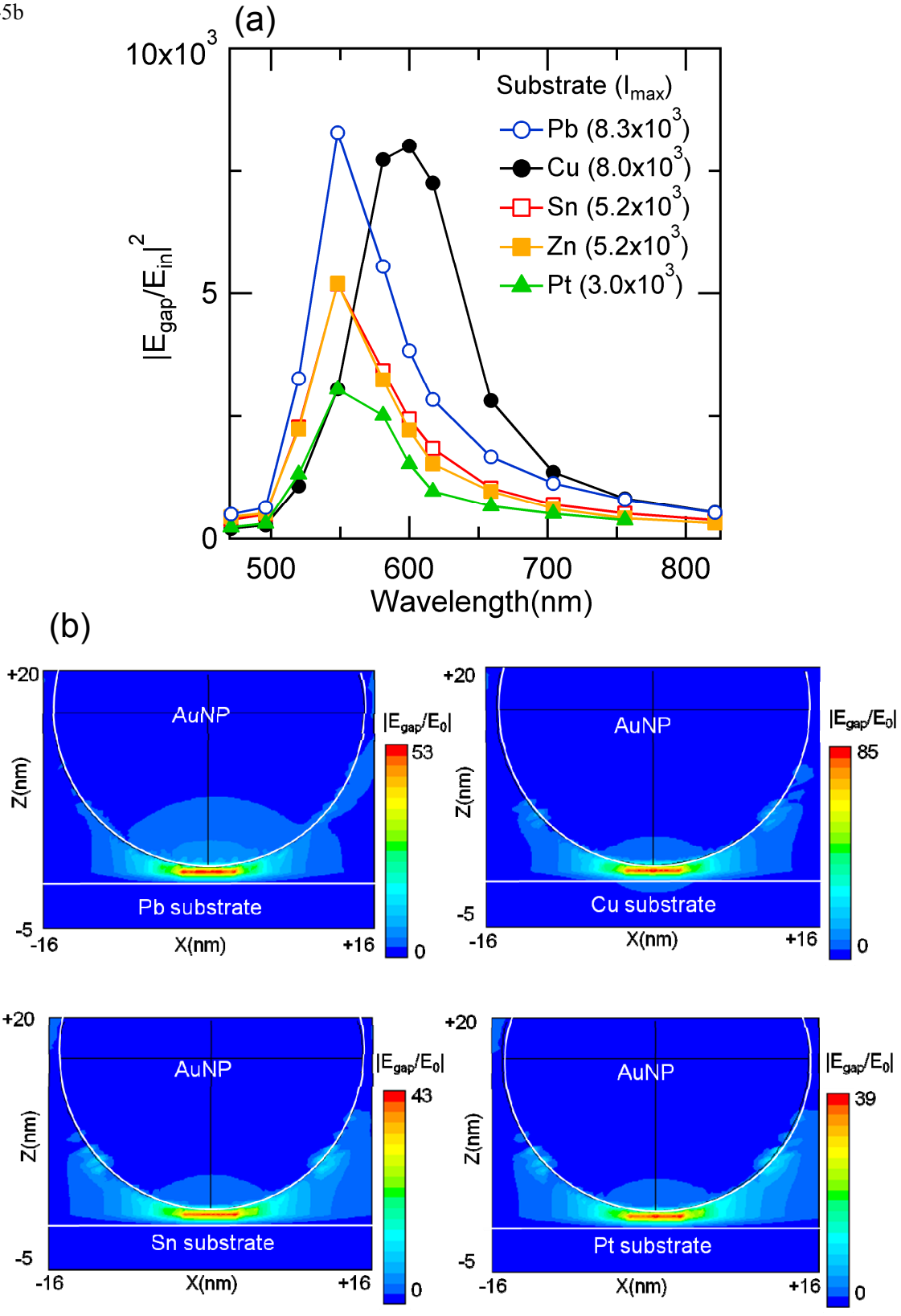

Fig. 6

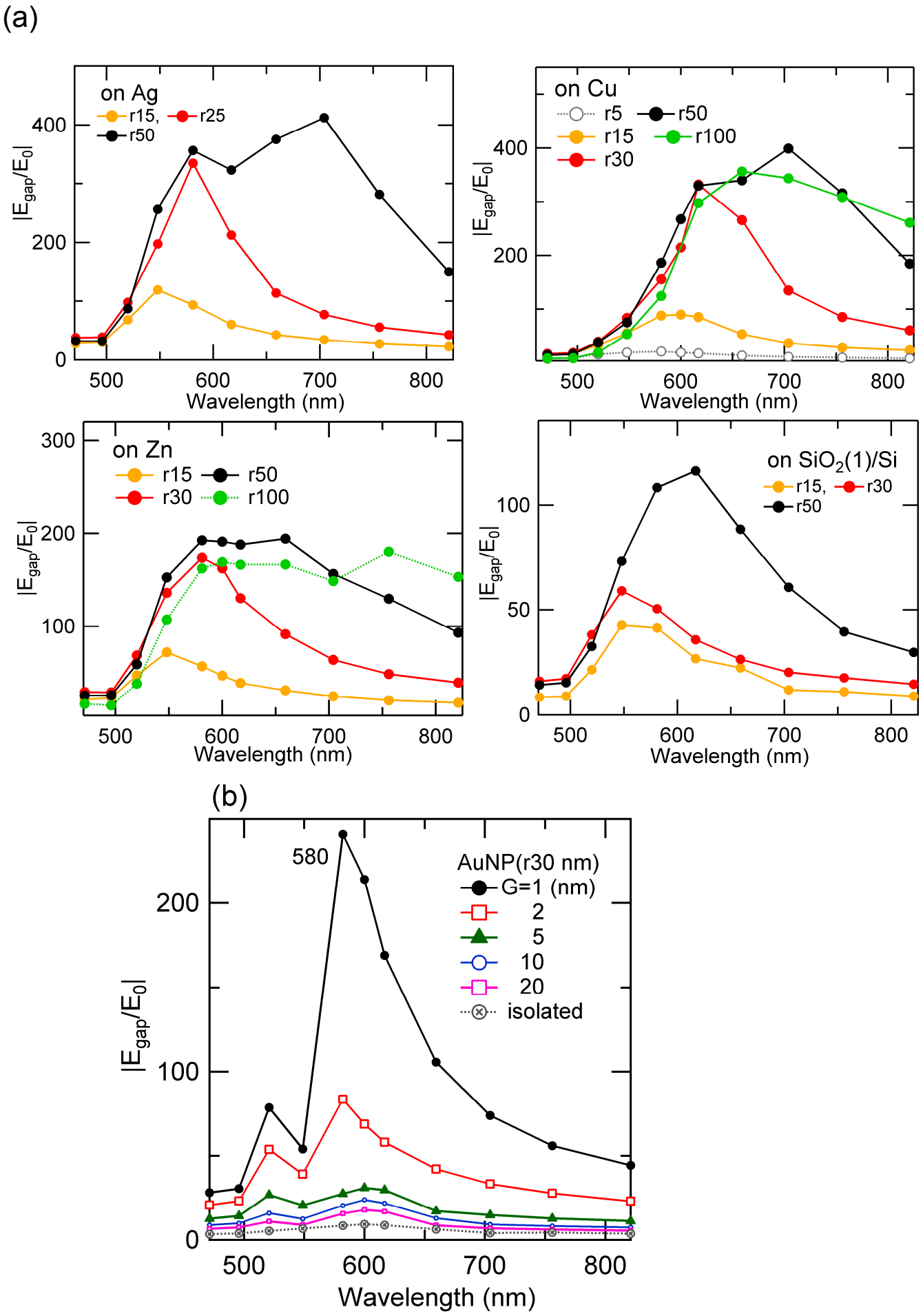

Fig. 7a-7b

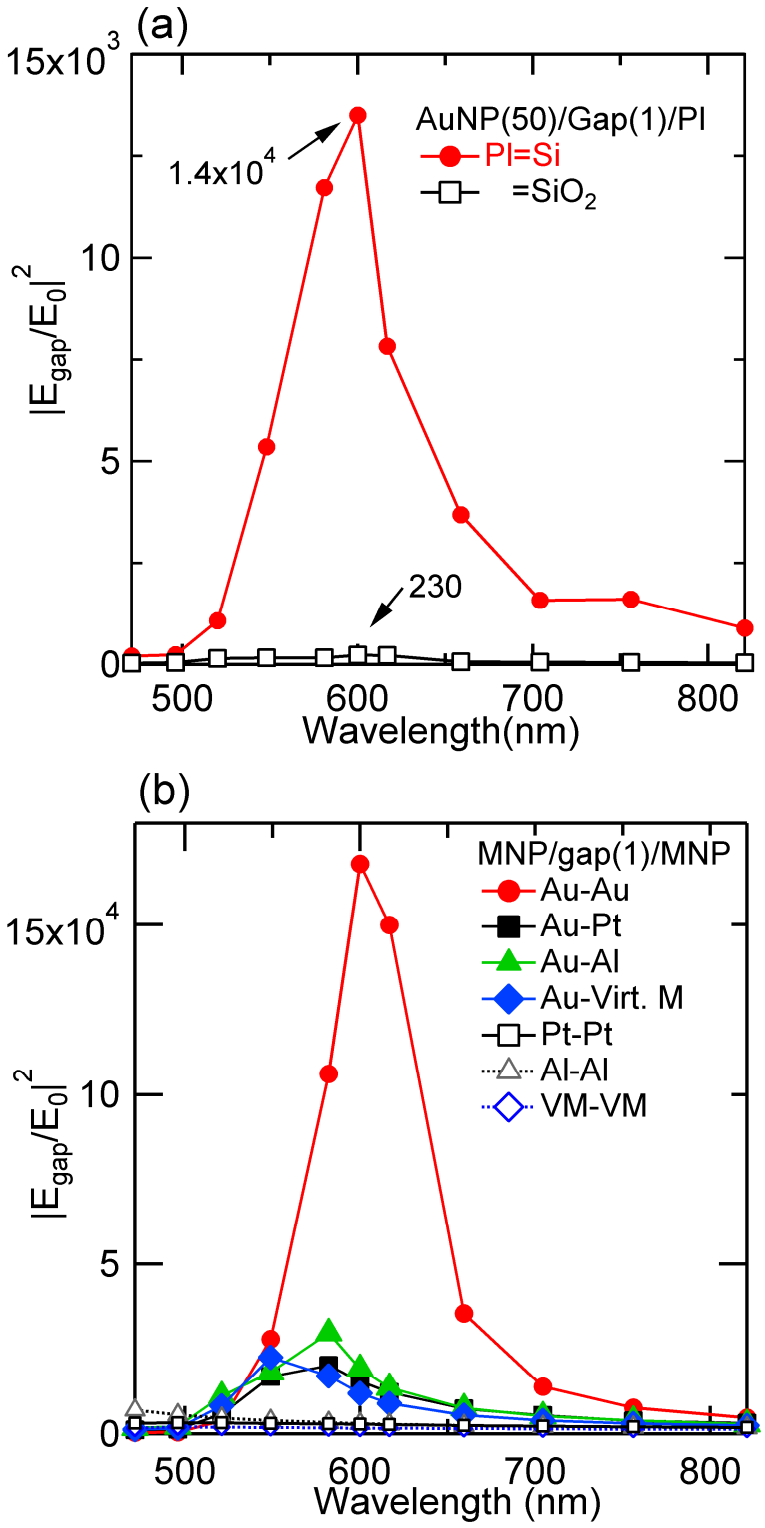

Fig. 8a-8f

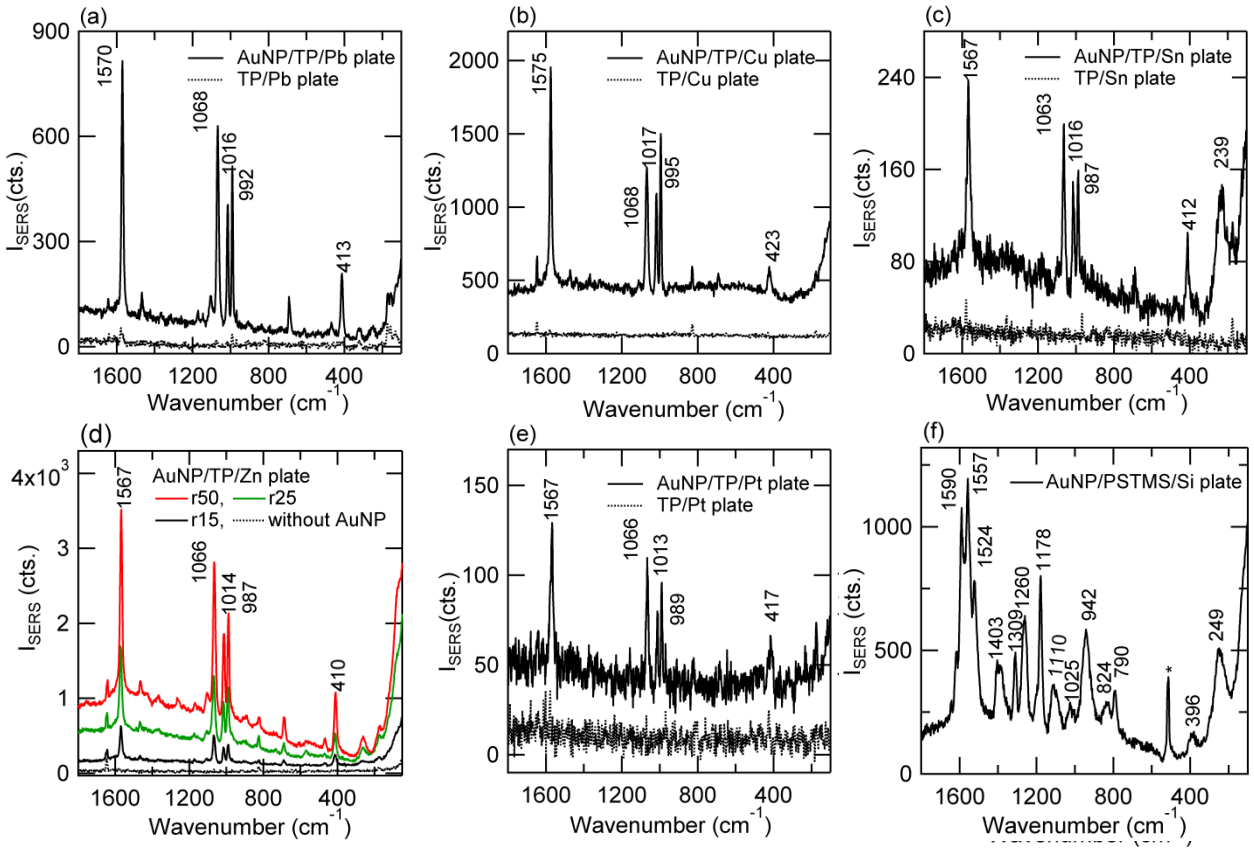

Fig. 9a-9d

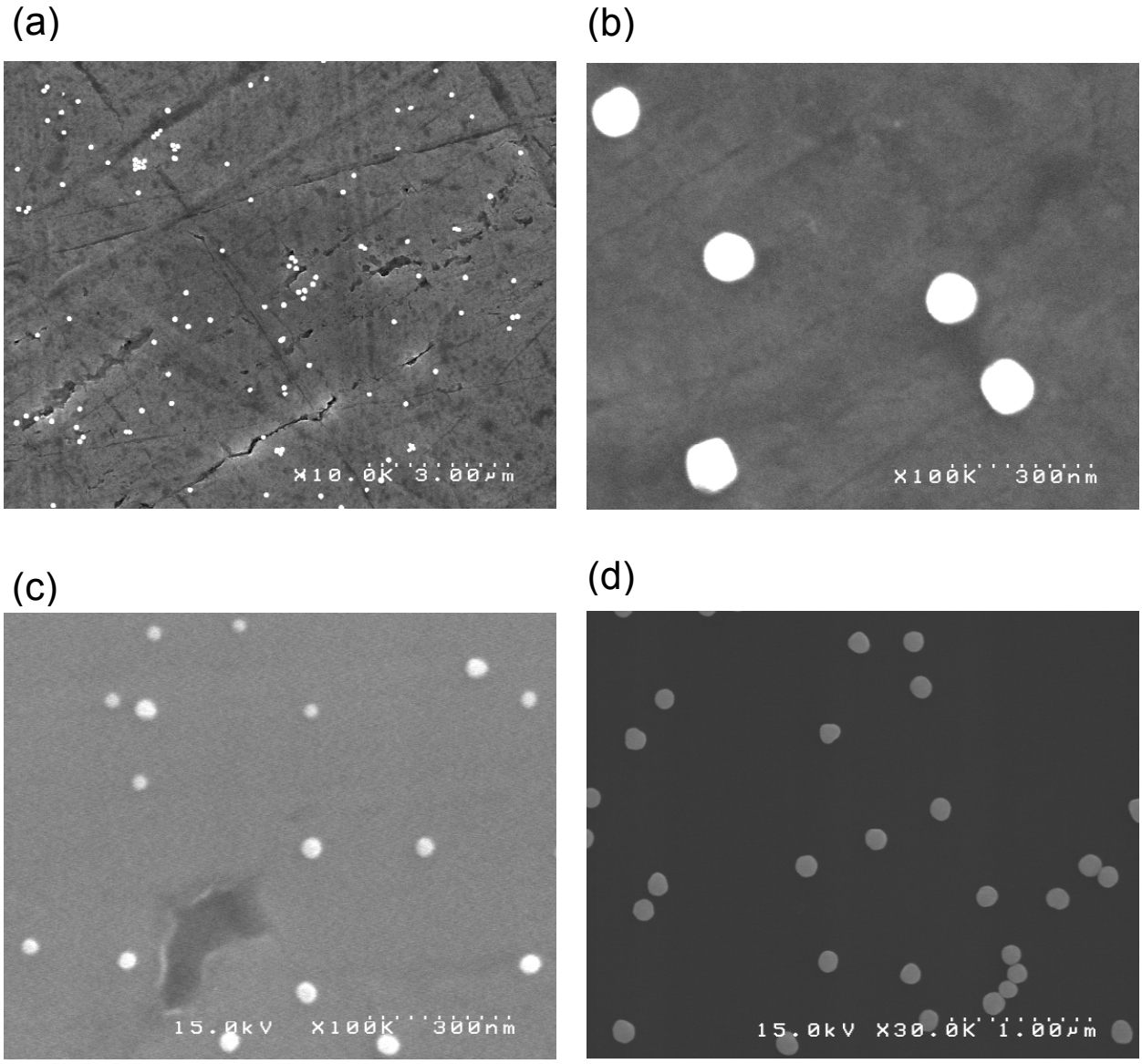

Fig. 10a-10d

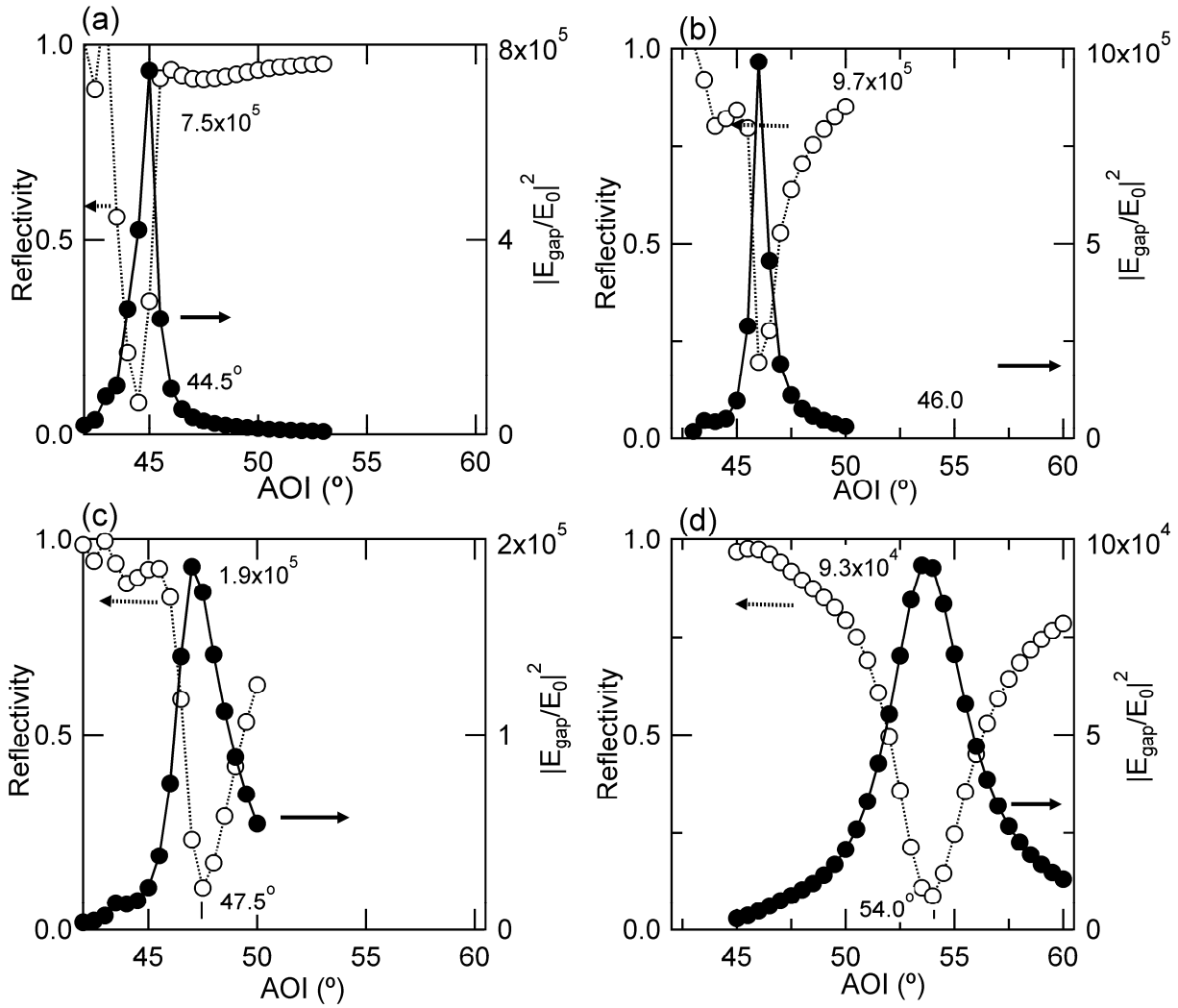

Fig. 11a-11d

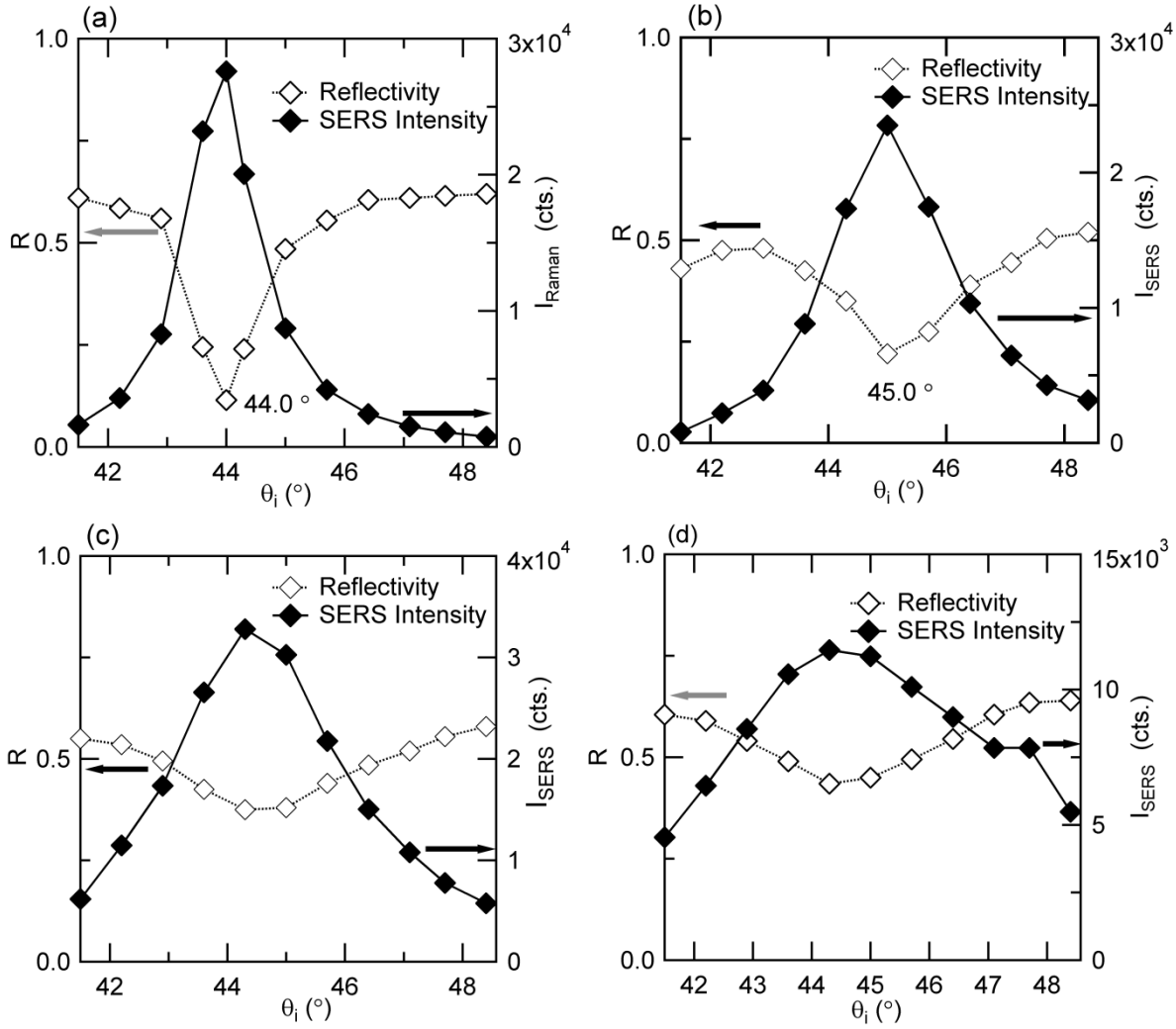

Fig. 12